SANDIA REPORT

SAND2014-16529
Unlimited Release
Printed August 2014

Simulation Studies of Nucleation of Ferroelectric Polarization Reversal

Geoff L. Brennecka and Benjamin Winchester

Prepared by
Sandia National Laboratories
Albuquerque, New Mexico 87185 and Livermore, California 94550

Sandia National Laboratories is a multi-program laboratory managed and operated by Sandia Corporation, a wholly owned subsidiary of Lockheed Martin Corporation, for the U.S. Department of Energy's National Nuclear Security Administration under contract DE-AC04-94AL85000.

Approved for public release; further dissemination unlimited.

Sandia National Laboratories

Issued by Sandia National Laboratories, operated for the United States Department of Energy by Sandia Corporation.

NOTICE: This report was prepared as an account of work sponsored by an agency of the United States Government. Neither the United States Government, nor any agency thereof, nor any of their employees, nor any of their contractors, subcontractors, or their employees, make any warranty, express or implied, or assume any legal liability or responsibility for the accuracy, completeness, or usefulness of any information, apparatus, product, or process disclosed, or represent that its use would not infringe privately owned rights. Reference herein to any specific commercial product, process, or service by trade name, trademark, manufacturer, or otherwise, does not necessarily constitute or imply its endorsement, recommendation, or favoring by the United States Government, any agency thereof, or any of their contractors or subcontractors. The views and opinions expressed herein do not necessarily state or reflect those of the United States Government, any agency thereof, or any of their contractors.

SAND2014-16529
Unlimited Release
Printed August 2014

Simulation Studies of Nucleation of Ferroelectric Polarization Reversal

Geoff L. Brennecka
Electronic, Optical, and Nanostructured Materials Department

Benjamin Winchester
Computational Materials & Data Science Department

Sandia National Laboratories
P.O. Box 5800, MS 1411
Albuquerque, NM 87185-1411

Abstract

Electric field-induced reversal of spontaneous polarization is the defining characteristic of a ferroelectric material, but the process(es) and mechanism(s) associated with the initial nucleation of reverse-polarity domains are poorly understood. This report describes studies carried out using phase field modeling of $LiTaO_3$, a relatively simple prototype ferroelectric material, in order to explore the effects of either mechanical deformation or optically-induced free charges on nucleation and resulting domain configuration during field-induced polarization reversal. Conditions were selected to approximate as closely as feasible those of accompanying experimental work in order to provide not only support for the experimental work but also ensure that additional experimental validation of the simulations could be carried out in the future. Phase field simulations strongly support surface mechanical damage/deformation as effective for dramatically reducing the overall coercive field (E_c) via local field enhancements. Further, optically-nucleated polarization reversal appears to occur via stabilization of latent nuclei via the charge screening effects of free charges.

Acknowledgment

This work was supported by the Physics and Engineering Models (P&EM) portion of the Advanced Simulation and Computing (ASC) Program and built upon earlier experimental work that was supported by the Laboratory Directed Research and Development (LDRD) program. The authors wish to express their appreciation to Veena Tikare (1444) and Corbett Bataille (1814) for assistance with code development and implementation, David Scrymgeour (1728) for technical discussions related to $LiTaO_3$ materials parameters and behavior, and Tom Buchheit (1814), Jeff Rodelas (1831), Mike Sinclair (1816), Fred Zutavern (5444), Gary Dension (5443), Gary Peña and Steve Glover (1353), and Larry Schneider (1350) for technical and/or financial assistance with the earlier experimental components that provided input and guidance for these simulation-focused efforts.

Contents

Nomenclature **9**

1 Introduction **11**

2 Phenomenological theory for ferroelectrics **13**

2.1 Landau Energy 13

2.2 Electrostatic Energy 14

2.3 Elastic Energy 15

2.4 Gradient Energy 16

3 Numerical details and model discussion **17**

3.1 Evolution equation 17

3.2 Electrostrictive parameters 17

3.3 Coercive field E_c 18

3.4 Background dielectric constant for $LiTaO_3$ 18

4 Indent-mediated ferroelectric switching in $LiTaO_3$ **19**

4.1 Motivation 19

4.2 Methodology 19

4.3 Results 21

4.4 Simulation details 22

5 Laser-mediated nucleation and switching in $LiTaO_3$ **23**

5.1 Part 1: Effects of bound charge centers on nucleation 25

5.2 Part 2: Stability of nuclei under an applied electric field 30

5.2.1 Methods 30

5.2.2 Results 31

6 Conclusions **33**

References **34**

Appendix

A Material parameters for $LiTaO_3$ **37**

List of Figures

2.1 Schematic double-well energy potential for $T < T_C$. 14

4.1 Previous experimental work showed that surface indentations significantly decreased the polarization reversal time for $LiTaO_3$ wafer samples. 20

4.2 More recent experimental work [1] demonstrated similarly-reduced switching times for surface-scratched $LiTaO_3$ crystal samples under high power drive conditions. . . 20

4.3 Speed of switching for various indent widths under a constant voltage ramp rate. . . 21

4.4 Speed of switching for varying magnitudes of extra potential applied at indent under a constant voltage ramp rate. 22

5.1 Data traces from a measurement in which a square wave just below the coercive voltage was applied to a $LiTaO_3$ single crystal showing enhanced charge release (presumed ferroelectric switching) upon illumination with 8 mW of 390 nm laser light. 24

5.2 Schematic illustration of charge screening in the nucleation, stability, and propagation of charged domain walls. 25

5.3 Graphical illustration of the basic approach to the simulations discussed here. 26

5.4 Comparison of $E_{applied}$ at first nucleation to the magnitude of charge center. 27

5.5 Comparison of $E_{applied}$ at first nucleation to the angles between the charge centers. 28

5.6 Minimum size of stable nuclei vs applied field, showing also the effect of changing the background dielectric constant, ε_b, which sets the electric field resulting from bound charge (such as at uncompensated domain walls). A larger ε_b means smaller resulting electric fields, and smaller stable nuclei. 32

List of Tables

4.1 Additional simulation parameters 22

Nomenclature

E_c Coercive field: the magnitude of electric field required to reverse polarization in a ferroelectric, generally defined as the point(s) on the Polarization vs. Electric field hysteresis loop where the loop crosses the P=0 axis.

HWHM Half-width half-maximum: one of several methods for describing a symmetric distribution, in this case, half of the width of the distribution at the value which is one half of the maximum value.

$LiNbO_3$ and $LiTaO_3$ Lithium Niobate and Lithium Tantalate: very similar ferroelectric materials with large remanent polarizations, small saturated permittivities, and low electromechanical response. These materials are commercially available in single crystal form and are commonly used in electro-optic devices. Their crystal structure precludes the existence of non-180° domain walls making them excellent subjects for fundamental studies of domain dynamics. The coercive fields of these crystals show an extremely strong dependence on Li stoichiometry.

SNL Sandia National Laboratories

TDGL Time Dependent Ginzburg-Landau: equation that describes the evolution of polarization as a linear relationship of the variational derivative of the energy functional with respect to polarization.

Chapter 1

Introduction

The fundamental phenomena associated with ferroelectric switching began receiving significant attention in the 1950s [2–5] and with the advent of advanced characterization and simulation tools has seen a recent resurgence in interest. [6–13] Many of the questions that continue to perplex the ferroelectrics community are associated with the process of initial nucleation of otherwise-oriented domains upon application of a switching electric field. The project whose results are described here was conceived to take advantage of the simulation capabilities and expertise available within SNL to develop a better understanding of the processes and critical parameters associated with the formation and stability of nuclei of inverse-polarity domains within a matrix of homogeneous polarization. Previous experimental work (some of which is described in an earlier SAND report [1]) demonstrated conclusively that mechanical surface damage could significantly affect polarization reversal times in single crystal ferroelectrics and hinted that optically-induced nucleation may also be possible; this project was structured in order to develop a simulation framework that could provide some theoretical support to these prior experimental findings and help to develop a more complete understanding of dynamic ferroelectric response under a variety of drive conditions.

This report begins with an brief overview of the phenomenological theory of ferroelectric materials as a way of introducing the terminology and energy-based arguments that form the basis of the rest of the work. As this work was entirely focused on simulation, the input material parameters came from literature values. Since an entirely self-consistent set of parameters were not available in the open literature, we used the best that we could find and discuss the concerns and rationale behind associated assumptions in Chapter 3; a full list of the material parameters used in this work can be found in Appendix A. Based on the earlier experimental work that prompted this study, the next two chapters, 4 and 5, address the role(s) of surface mechanical damage and optical energy, respectively, in nucleation of reverse-polarity domains. The code developed for this work is available by contacting Amy Sun, manager of 1814 (acsun@sandia.gov).

Chapter 2

Phenomenological theory for ferroelectrics

We derive an energy functional F for the system as a function of strain, electric field, and polarization, and find the temporal evolution of the system by the time-dependent Ginzburg-Landau (TDGL) equation, which describes the evolution of the polarization, P_i, as a linear relationship of the variational derivative of the free energy functional with respect to the P_i,

$$\frac{\partial P_i}{\partial t} = -L\frac{\delta F[P,E,\varepsilon]}{\delta P_i}$$

The above can be thought of as finding the change in P_i that most quickly decreases the free energy of the system. Here we define the system free energy as the volume integral of the Landau, elastic, electrostatic, and gradient energies over the entire system [14],

$$F = F[P,E,\varepsilon] = \int f_{Landau} + f_{elastic} + f_{electrostatic} + f_{gradient} dV,$$

A brief discussion of the different energy terms follows.

2.1 Landau Energy

Landau theory allows us to describe the free energy in terms of a Taylor expansion of the order parameter near the critical temperature. For a second-order phase transition, as we go below the critical temperature, the second-order term becomes negative, creating a double-well potential or more, depending on the crystal symmetry (Figure 2.1). Here we discuss a Landau free energy estimate for materials in the $3m$ point group, such as $LiTaO_3$ and $LiNbO_3$. We denote the uniaxial crystallographic direction as the x_3 axis.

The 4th-order $\bar{3}m$ local Landau free energy is given as:

$$f_{Landau} = \alpha_1(P_1^2 + P_2^2) + \alpha_3 P_3^2 + \alpha_{33} P_3^4$$

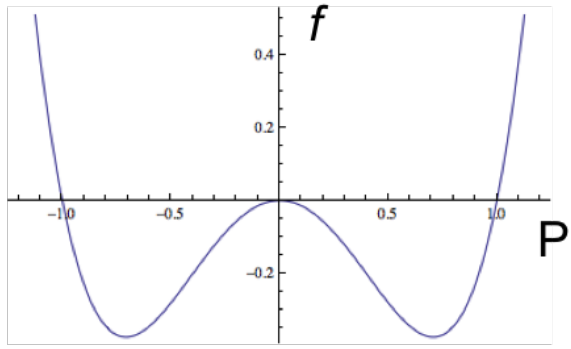

Figure 2.1. Schematic double-well energy potential for T $<$ T$_C$.

Where $\alpha_1 > 0$ as dictated by the lack of spontaneous polarization along the x_1 or x_2 axes. If $F_{Landau} = F_L$ represents the volume integral of the local free Landau energy, f_{Landau}, then the variational derivatives with respect to each P_i are given as:

$$\frac{\delta F_L}{\delta P_i} = \frac{\partial f_{L4}}{\partial P_i}$$

For P_1 and P_2 this simplifies as:

$$\frac{\delta F_L}{\delta P_1} = 2\alpha_1 P_1 \frac{\delta F_L}{\delta P_2} = 2\alpha_1 P_2$$

And for P_3, in factorized form:

$$\frac{\delta F_L}{\delta P_3} = P_3(2\alpha_3 + 4\alpha_{33}P_3^2)$$

2.2 Electrostatic Energy

In the case of a ferroelectric, the electrostatic energy can be written as: [15]

$$f_{electrostatic} = -\frac{1}{2}\varepsilon_0\varepsilon_{b,ii}E_iE_i - E_iP_i$$

Where E_i is the electric field along the x_i, P_i is the polarization along x_i, and ε_0 and $\varepsilon_{b,ii}$ are the electric constant and background dielectric constants, respectively. The variational form of the electrostatic energy with respect to polarization is simply:

$$\frac{\delta F_{electrostatic}}{\delta P_3} = -E_i$$

We recall that the potential, ϕ, and electric field, E_i are connected via

$$E_i = -\frac{\partial \phi}{\partial x_i}$$

So, describing the energy functional as a function of polarization and potential, we arrive at:

$$F[\mathbf{P}(x), \phi(x)] = \int \sum_i^{1,2,3} -\frac{1}{2}\varepsilon_0 \varepsilon_{b,ii} \frac{\partial \phi}{\partial x_i}\frac{\partial \phi}{\partial x_i} + P_i \frac{\partial \phi}{\partial x_i} dV$$

If we find the Euler-Lagrange equations associated with the variational derivative with respect to $\phi(x)$, we find, of course, the following equations:

$$\frac{d}{dx_i}\left(\varepsilon_0 \varepsilon_{b,ii} \frac{\partial \phi}{\partial x_i}\right) - \frac{dP_i}{dx_i} = 0,$$

If we assume that $\varepsilon_{r,ii}$ is spatially homogeneous, we can reformulate this as:

$$\frac{\partial^2 \phi}{\partial x_i^2} = \frac{\bigtriangledown \cdot P}{\varepsilon_0 \varepsilon_{b,ii}}$$

Or, since the bound charge is defined here as $\rho_b = -\bigtriangledown \cdot P$, we can put this in its common form, Poisson's equation:

$$\bigtriangledown^2 \phi = \frac{-\rho_b}{\varepsilon_0 \varepsilon_{b,ii}}$$

So Poisson's equation can be derived as the Euler-Lagrange equations of the electrostatic energy *e.g.*, by setting the first variational derivative of the electrostatic energy equal to zero.

2.3 Elastic Energy

We take a linear approximation to the elastic strain energy, given as:

$$
\begin{aligned}
f_{elastic} &= \frac{1}{2}c_{ijkl}e_{ij}e_{kl} = \frac{1}{2}c_{ijkl}(\varepsilon_{ij}-\varepsilon^0_{ij})(\varepsilon_{kl}-\varepsilon^0_{kl}) \\
&= \frac{1}{2}c_{ijkl}\left[\frac{1}{2}\left(\frac{\partial u_i}{\partial x_j}+\frac{\partial u_j}{\partial x_i}\right)-\varepsilon^0_{ij}\right]\left[\frac{1}{2}\left(\frac{\partial u_k}{\partial x_l}+\frac{\partial u_l}{\partial x_k}\right)-\varepsilon^0_{kl}\right]
\end{aligned}
$$

Where u_i is the ith component of mechanical displacement, e_{ij} is the elastic strain, c_{ijkl} is the elastic stiffness tensor, and ε^0_{ij} represents the eigenstrain. We also describe the total strain, ε_{ij},

$$
\varepsilon_{ij} = \frac{1}{2}\left(\frac{\partial u_i}{\partial x_j}+\frac{\partial u_j}{\partial x_i}\right),
$$

and the eigenstrains are connected to the polarizations via the electrostrictiver properties of the material,

$$
\varepsilon^0_{kl} = Q_{klop}P_oP_p.
$$

As with the electric potential, the mechanical displacement can be solved either via variational methods or directly.

2.4 Gradient Energy

The local gradient energy of polarization can be expressed in cubic form as

$$
\begin{aligned}
f_{Gradient} = &\frac{1}{2}g_{11}(P^2_{1,1}+P^2_{2,2}+P^2_{3,3}) + g_{12}(P_{1,1}P_{2,2}+P_{1,1}P_{3,3}+P_{2,2}P_{3,3}) \\
&+ g_{44}([P_{1,2}+P_{2,1}]^2+[P_{1,3}+P_{3,1}]^2+[P_{2,3}+P_{3,2}]^2) \\
&+ g'_{44}([P_{1,2}-P_{2,1}]^2+[P_{1,3}-P_{3,1}]^2+[P_{2,3}-P_{3,2}]^2)
\end{aligned}
$$

Where $P_{i,j} = \frac{\partial P_i}{\partial x_j}$, and $P_i, P_{i,j}$, and the gradient energy coefficients g_{ij} may in a general form all be functions of position. However, here we assume that the gradient energy coefficients are isotropic and uniform in space; $g_{11} = 2g_{44} = 2g'_{44}$, and $g_{12} = 0$. With spatially homogeneous gradient energy coefficients, the local variational derivatives with respect to P_i are:

$$
\frac{\delta f_G}{\delta P_i} = \frac{d}{dx_j}\frac{\partial f_G}{\partial P_{i,j}}.
$$

Chapter 3

Numerical details and model discussion

3.1 Evolution equation

In solving the TDGL equation, we treat the gradient energy implicitly, as doing so greatly increases the simulation numerical stability. Defining F_{ng} as the non-gradient energy terms, the resulting discretization of the TDGL equation is as follows:

$$\frac{P_i^{n+1}}{\Delta t} + L\frac{\delta F_{gradient}(P_i^{n+1})}{\delta P_i^{n+1}} = -L\frac{\delta F_{ng}[P_i^n, E, \varepsilon]}{\delta P_i^n} + \frac{P_i^n}{\Delta t}$$

where P_i^n refers to the polarization P_i at timestep n.

3.2 Electrostrictive parameters

The material parameters for $LiTaO_3$ and $LiNbO_3$ come from the seminal work by Scrymgeour, Gopalan, *et al.* [16] In this work, we were unable to derive a robust, consistent set of values for the electrostrictive coefficients Q_{klop} from the given coefficients in the paper. We found disagreements between the stated values for the elastic stiffness constants and the values derived from them, and we were unable to reconcile the derivation of the simplified energy terms used in their formulas with any standard model for calculating free energy based on strain. We therefore set the electrostrictive coefficients to zero, and the elastic energy effects are neglected. While at first this may seem to be an unjustifiable oversimplification, since $LiTaO_3$ and $LiNbO_3$ have only two antiparallel polarization directions, ferroelastic contributions are non-existent. It is known that the 180° domain walls in these materials are not entirely strain-free, [17–19] but given the constraints, we chose to investigate the limiting case dominated by electrostatic effects rather than assuming arbitrary non-zero values for the electrostrictive parameters and thereby effectively investigating as less-well-defined situation.

3.3 Coercive field E_c

The coercive electric field, E_c, is defined as the electric field under which the ferroelectric polarization switches. Given the parameters used here (listed in Appendix A), the coercive field for a nucleation-free, defect-free system is 0.262 MV/m. This value is roughly 3-4 orders of magnitude greater than the experimental value(s), as is common for estimates of E_c based solely on Landau theory. Two of the potential explanations for an overly-high estimate of E_c will be relevant for this work: nucleation sites [20, 21] and charge screening of depolarization fields. [22]

3.4 Background dielectric constant for $LiTaO_3$

The best-known Landau parameters for $LiTaO_3$ and $LiNbO_3$ employ a dielectric constant of about 45. [16] However, typical background dielectric constant values for similar ferroelectrics are in the range of 6-15. Additionally, common practice used to be to employ the relative dielectric constant in the calculation of Landau parameters instead of the background dielectric constant. These factors lead the authors to suspect that the background constant referenced and employed here is too high by a factor of 3-4x. However, properly demonstrating this would require a re-analysis of the literature work which is outside the scope of this study, so for now, we use the literature data with full awareness of the potential shortcomings.

Chapter 4

Indent-mediated ferroelectric switching in $LiTaO_3$

4.1 Motivation

Here, we consider a physical method for introducing nucleation sites, a ferroelectric with mechanical indents on the surface. Former experimental work indicates that indents and/or scratches on the ferroelectric surface increase the switching uniformity and rate (Figures 4.1 and 4.2), presumably by increasing the number and spatial uniformity of nucleation sites.

The full scope of the resulting materials property changes from a mechanical indent is unclear we would expect the indent to result in a buildup of dislocations, ion displacement, etc., any of which might contribute to the nucleation and pinning properties of the ferroelectric. However, the indent also provides a change in the surface topography of the ferroelectric. By depositing an electrode onto the ferroelectric surface, the electrode inherits the sharp topography change, protruding into the sample and resulting in an increased local electric field under an applied bias.

4.2 Methodology

We model the effects of indents on $LiTaO_3$ as an increased potential distribution on the top surface of the ferroelectric. Using fixed-potential boundary conditions, we break the applied bias into two parts, the uniform bias ϕ_u and the heterogenous "overpotential" resulting from the indent, $\phi_n(x)$, such that the resulting top-surface potential ϕ_{top} is given as:

$$\phi_{top}(x) = \phi_u[1 + \phi_n(x)].$$

We employ a Lorentzian distribution to set the shape of the overpotential,

$$\phi_n(x) = I\left(\frac{\gamma^2}{(x - x_0)^2 + \gamma^2}\right)$$

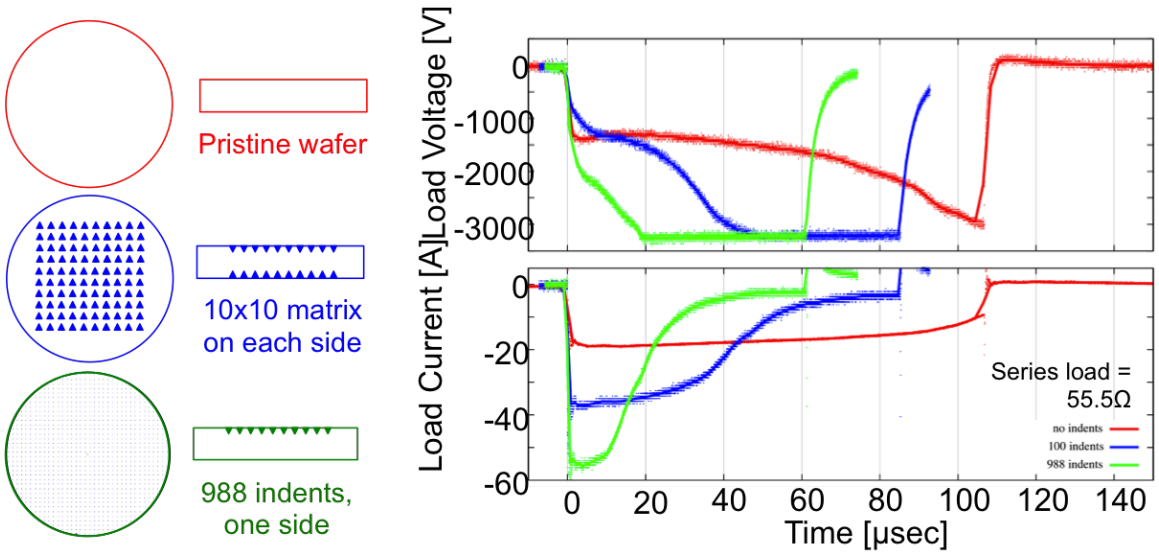

Figure 4.1. Previous experimental work showed that surface indentations significantly decreased the polarization reversal time for $LiTaO_3$ wafer samples.

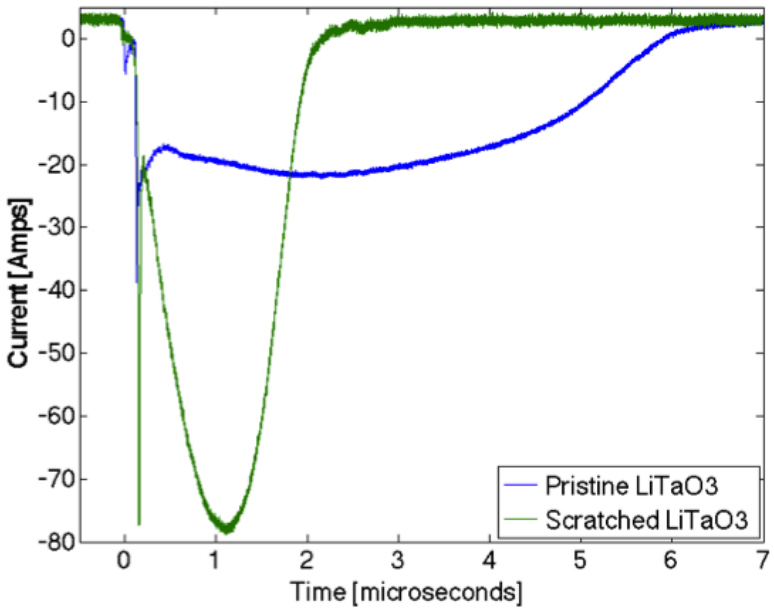

Figure 4.2. More recent experimental work [1] demonstrated similarly-reduced switching times for surface-scratched $LiTaO_3$ crystal samples under high power drive conditions.

Where I is the peak height of the distribution, γ is the half-width half-maximum (HWHM), and x_0 represents the spatial location of the Lorentzian peak. The above equations imply that the indent bias adds a fixed percentage scaling to the uniform bias. We vary the HWHM and the distribution magnitude, and examine the effects on speed of switching. We start with no applied top surface bias, and gradually ramp up ϕ_u at a rate of 0.1 every 200 timesteps, while the bottom surface is held fixed with zero potential.

4.3 Results

We present the results in terms of what percent of the opposing electrode area has switched.

In Figure 4.3 we present the effect of changing γ for a given peak overpotential, I, of 30%. The base applied field refers to the electric field calculated from just ϕ_u. We note that initial curves all rise together to about 150kV/m before diverging; this is a numerical artifact coming from polarization change under the applied field across the entire sample and should not be interpreted to mean that nucleation has occurred.

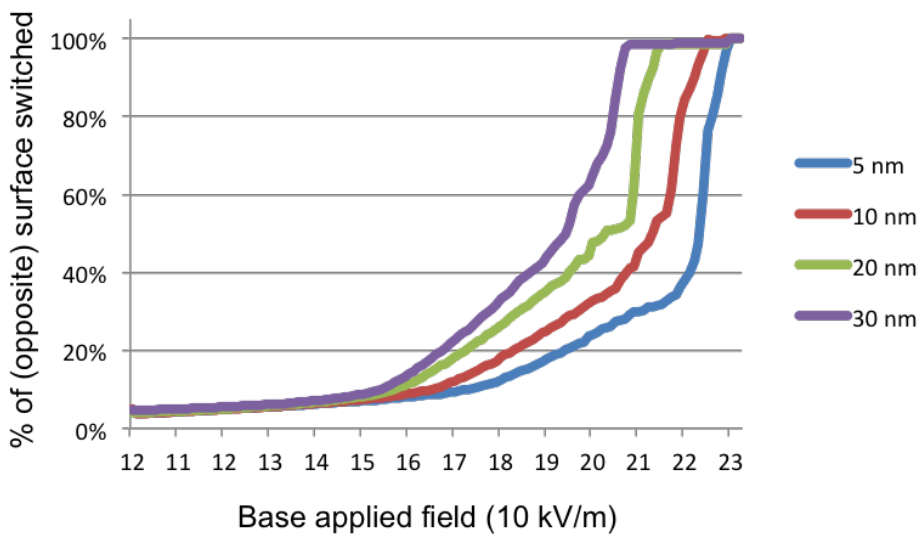

Figure 4.3. Speed of switching for various indent widths under a constant voltage ramp rate.

We see that the wider indents nucleate faster than the narrower indents, and with proportionally more initial surface area, they also grow faster at a given applied field. For each of the indents, we note that there is an applied field where growth sharply accelerates. The mechanics of this are unknown.

In Figure 4.4 we present the effect of changing the overpotential magnitude while using an indent width of 10nm. As might be expected, a greater potential increase results in nucleation

at a lower applied field. However, the switching occurs at about the same rate, regardless of the overpotential size. The exception, of course, is the reference case with zero overpotential, which matches the analytical expectation of abrupt, homogenous switching.

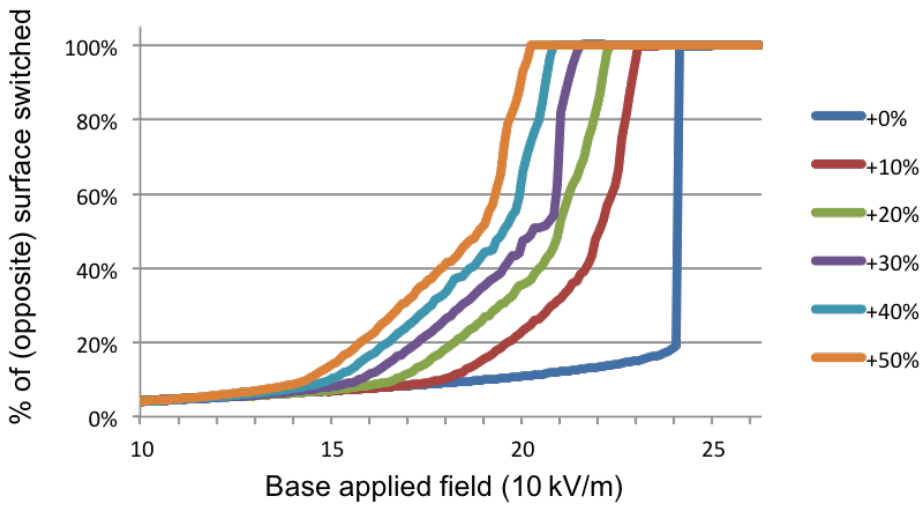

Figure 4.4. Speed of switching for varying magnitudes of extra potential applied at indent under a constant voltage ramp rate.

4.4 Simulation details

These are 2-D simulations, with a system size of 64nm by 125nm, along x_1 and x_3 respectively, with two gridpoints for every nanometer of real space. The initial domain structure is just a single domain of $+P_3$. The material parameters for $LiTaO_3$ can be found in Appendix A, and all other simulation parameters are given in table 4.1.

Table 4.1. Additional simulation parameters

Δt	0.2
ε_b	44.9
g_{11}	4.56

Chapter 5

Laser-mediated nucleation and switching in $LiTaO_3$

Figure 5.1 shows one example of the data collected as part of earlier experimental efforts which suggested that optical energy could be used to assist with ferroelectric switching in $LiTaO_3$. Additional experiments ruled out this being a simple effect of photocurrent generation, and the null results from high power infrared (IR, 780 nm) illumination strongly suggests that this is not simply a thermal effect. Several literature studies have also indicated that lasers can be used to either promote [23, 24] or inhibit [25] polarization reversal, and a birefringence laser pattern can be used to pattern a domain structure within an optically-transparent ferroelectric. [26] One goal of the present simulation-focused work was the investigate the potential mechanisms and their relative contributions to polarization reversal.

There are two potential mechanisms by which application of laser light can induce or encourage domain switching. The first is that the laser application sets up regions with alternating, high electric field. [23] In order to minimize electrostatic energy, the ferroelectric polarization lines up with the laser-induced electric field. Alternatively, slow-moving free charges may move to screen the laser-induced fields, and upon removal of the laser light, these charges induce an electric field that switches the polarization.

The second mechanism involves the excitation of electrons or holes, raising the amount of mobile charge. [22, 26, 27] Given that a switched domain wall has a high concentration of bound charge due to the head-to-head or tail-to-tail orientation of the polarization, these free charges may serve to screen the electrostatic energy associated with the domain wall, encouraging domain nucleation (Figure 5.2).

Both mechanisms have supporting evidence. We use the phase-field model to examine both mechanisms separately, although the two mechanisms are not necessarily mutually exclusive and joint consideration is an obvious subject for future work. In Part 1, we introduce bound charge centers in order to examine the effects of regions of concentrated electric fields. In Part 2, we investigate the stability of a nucleus with respect to a given applied electric field.

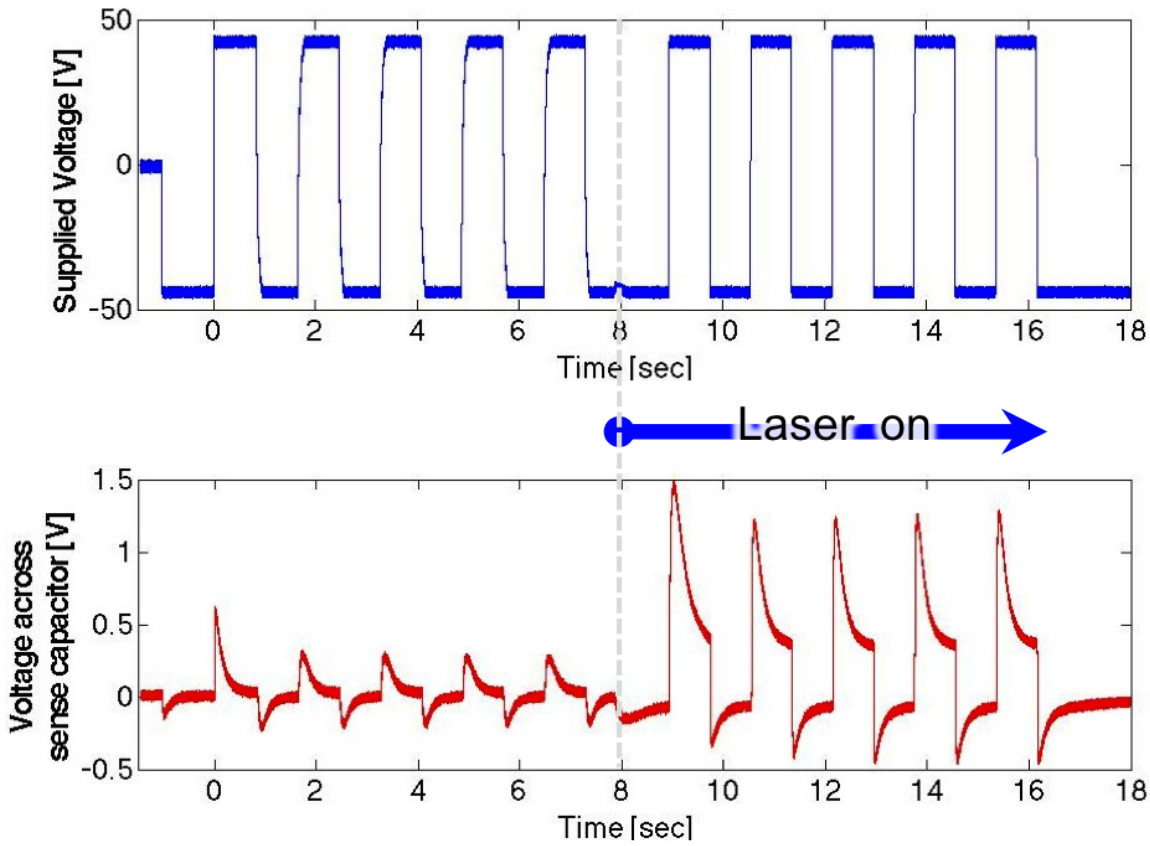

Figure 5.1. Data traces from a measurement in which a square wave just below the coercive voltage was applied to a $LiTaO_3$ single crystal showing enhanced charge release (presumed ferroelectric switching) upon illumination with 8 mW of 390 nm laser light.

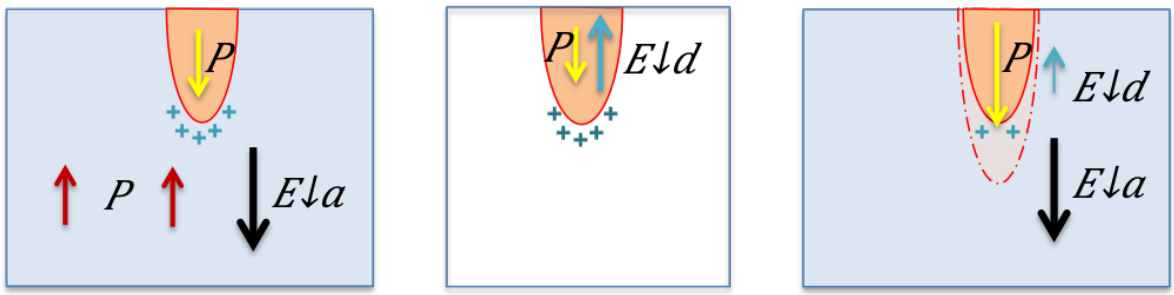

(a) Under an applied field, new domains can nucleate but have highly charged domain walls

(b) Charged domain walls create a depolarization field E_d that cancels the applied field and suppresses the new domain.

(c) Reducing the net bound charge at the domain wall reduces the depolarization field, and allows the new domain to grow.

Figure 5.2. Schematic illustration of charge screening in the nucleation, stability, and propagation of charged domain walls.

5.1 Part 1: Effects of bound charge centers on nucleation

Beginning with a simulation of a uniform, poled, bulk single crystal of $LiTaO_3$, we introduce temporally-fixed charge centers of varying distance, angle, and magnitude, in order to identify the effects of a spatially-varying electric field on the ferroelectric. We employ one positive and one negative charge center of equal magnitude and shape. To set the shape, we use a Lorentzian distribution, with a constant HWHM of 5nm across all simulations considered here, and we vary the angle between positive and negative charge centers, such that the resulting electric field varies between being parallel and perpendicular to the applied electric field (Figure 5.3). Once the charge center positions and magnitudes are set, we slowly increase the applied electric field along x_3 until nucleation is observed.

Let us denote the applied field at first nucleation as E_n, the angle between charges as $\rho\theta$, the distances between charge centers as ρ_d, and the peak magnitude of the charge centers ρ_{mag}. In a simple 1-D case with charge centers aligned along x_3, alternating regions of positive and negative charge produce an electric field with alternating sign, and this gives simplistic results: when the resulting electric field plus the applied field becomes larger than E_c anywhere, nucleation results.

Let us consider a 2-D simulation, with simulation details given below. In Figure 5.4, we show the applied electric field required for nucleation, E_n, as we vary both the distance between the charges and the peak magnitude. At low magnitudes ($\rho_{mag} = 0.01$), neither $\rho\theta$ nor ρ_d matters much, and E_n is close to E_c. As we increase the charge center magnitude, we notice a few trends. The required field drops for all angles and distances, but at unequal rates. Nucleation is always easiest when the charge centers are aligned with the applied electric field, when $\rho\theta$ is low. Last, when $\rho\theta$ and ρ_{mag} are both high, nucleation is harder to obtain as the charge centers move closer together, in contrast to most of the cases where nucleation becomes easier as the charges move

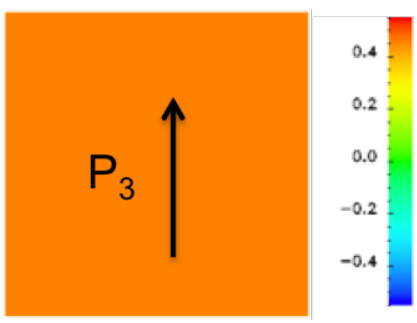

(a) Take a uniform, bulk ferroelectric

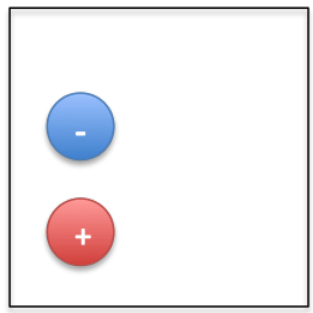

(b) add some bound charge distribution

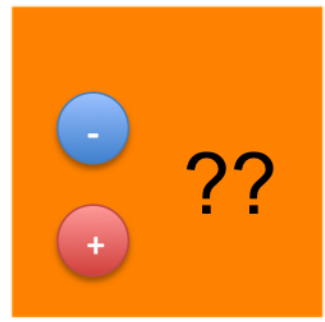

(c) and observe the effects on nucleation, switching, domain growth, etc.

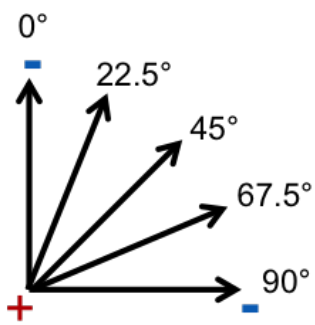

(d) Vary: angle between charges

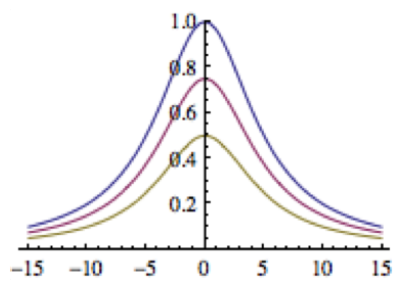

(e) amount of charge

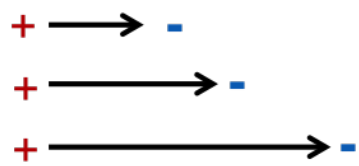

(f) and distance between charges: (50, 100, 150, 200, 250, 300 nm)

Figure 5.3. Graphical illustration of the basic approach to the simulations discussed here.

closer together.

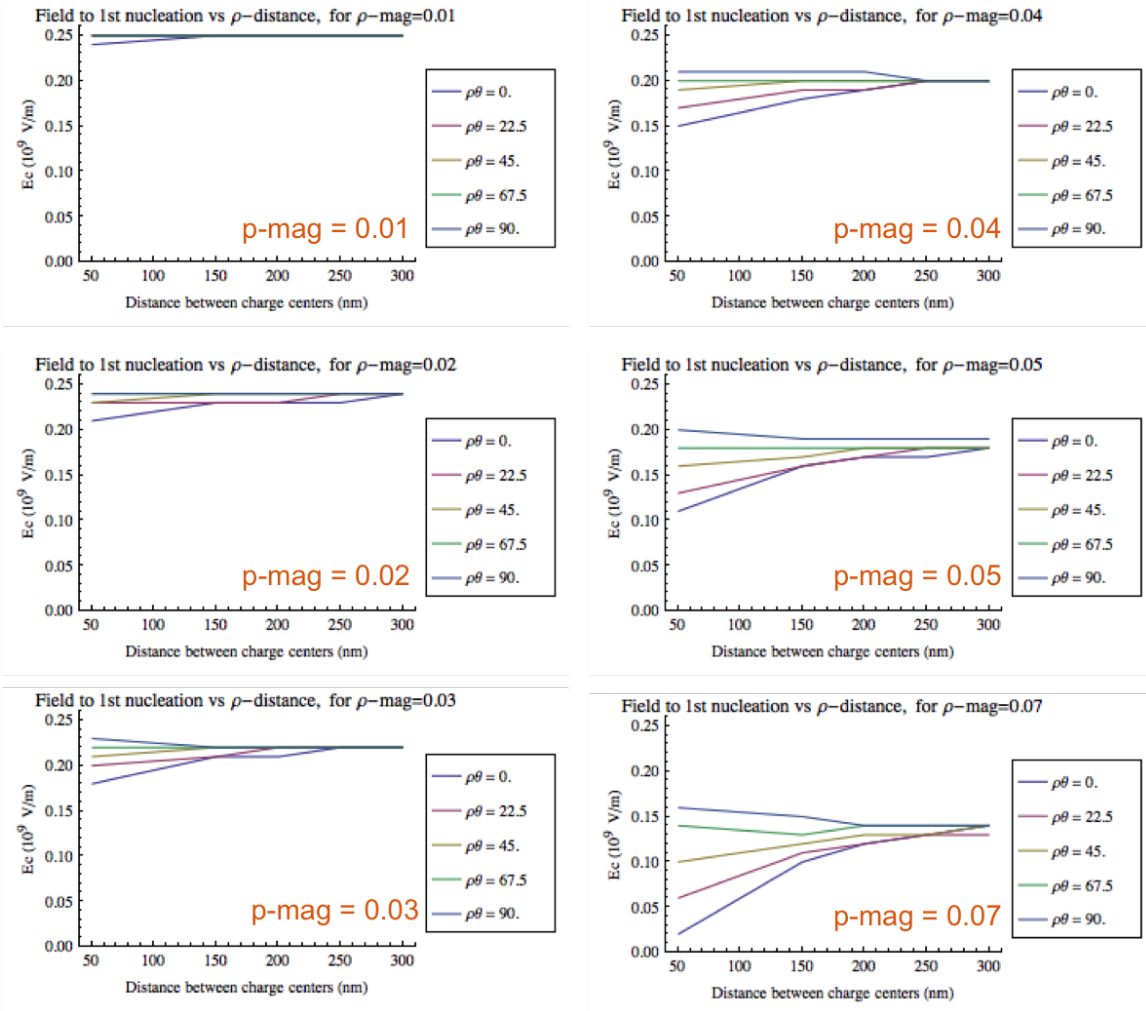

Figure 5.4. Comparison of $E_{applied}$ at first nucleation to the magnitude of charge center.

In Figure 5.5, we present the same data, organized around ρ_{mag} instead of $\rho\theta$. We note again that both ρ_d and ρ_{mag} have the greatest effect on E_n when $\rho\theta$ is low.

We would like to note that the above analysis only addresses the ease of nucleation, not how quickly the domains grow. A cursory analysis of the switching behavior (not shown here) suggests that while nucleation is easiest when charge centers are aligned with the electric field, nucleated domains grow fastest when the charge centers are misaligned. This has a few plausible explanations:

1. Misaligned charge centers have a greater lateral component to the electric field, which may induce the domains to grow more quickly laterally.

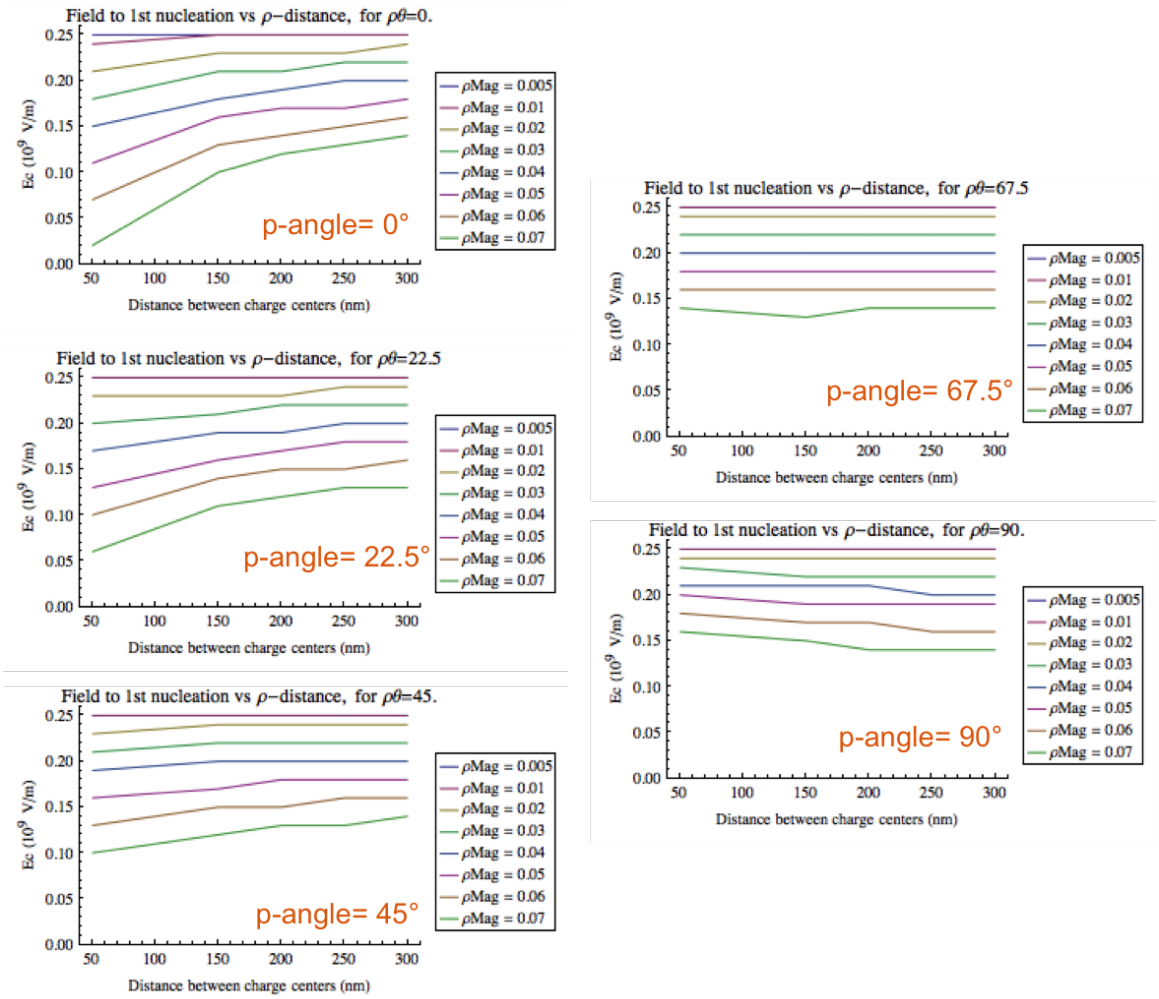

Figure 5.5. Comparison of $E_{applied}$ at first nucleation to the angles between the charge centers.

2. Analogous to the decreased switching time for larger physical nucleation sites from Figure 4.3, charge centers at large angles with respect to the applied field will present a larger effective cross-sectional area. Since domain growth along the polarization direction is known to occur much more quickly than lateral domain growth, increasing the area of each normal-growth domain reduces the amount of lateral domain wall motion required.

3. With misalignment, E_n is higher, and domains always grow faster under higher applied fields. In this case, the quicker growth after nucleation would be simply an artifact of the higher nucleation field.

4. Charge centers emit electric field in all directions. Where the resulting electric field is in the same direction as the applied field, nucleation is enhanced, and where it opposes the applied field, both nucleation and switching are suppressed. Aligning charges produces a higher nucleating field, but also aligns the nuclei in such a way that switching will be hindered by the opposing electric fields on the unfavorable side of the charge center.

We would like to point out that both quickly-growing and slowly-growing nuclei may have practical uses for rapid and uniform ferroelectric switching. If indeed nuclei can be induced and pinned by laser-induced charge distributions, we might try to establish a regular, optimal distribution of non-growing nuclei under an applied laser illumination, then switch the illumination off to allow those domains to move freely, prompting quick and controllable switching of the material. On the other hand, if other, unexpected nucleation sites prove to play an important role in switching, we may not be able to restrict the growth of the nuclei, leading to irregular and diffuse switching. In this case, the best switching properties might come from inducing as many quickly-growing nuclei as possible.

Last, we note that a charge center of $\rho_{mag} = 0.05$ with a HWHM of 5nm correlates to an approximate charge density of 10^{16} C/m^3, too high to be physically realistic. This would suggest that charge centers cannot be, by themselves, the mechanism inducing nucleation and switching in laser illumination of $LiTaO_3$. However, the extremely high charge concentration that is needed for nucleation may also just be another result of the Landauer Paradox, the discrepancy between theory and experiments on the critical field needed for switching.

We used 2-D simulations, with a system size of 600nm x 600nm and 600 x 600 gridpoints on a fixed, regular mesh. The timestep is taken as $\Delta t = 0.06$, which does not yet have a physical meaning without an experimental comparison for calibration of L, the kinetic parameter. We begin the simulations with a uniform polarization of $P_1 = P_2 = 0$; $P_{=}0.1$ C/m^2 and no applied electric field. We allow the simulations to come to equilibrium over 600 timesteps before we introduce the charge centers or start to change the applied electric field. We introduce the charge centers at 600 timesteps, and at 900 timesteps we begin lowering the applied electric field along x_3 by 0.01 MV/m every 200 timesteps. This interval of timesteps seems to be large enough to allow most metastable behavior to settle out and for the simulation to get close to the pseudo-static conditions.

5.2 Part 2: Stability of nuclei under an applied electric field

Here we endeavor to find the smallest stable nuclei for a given an applied electric field. This data serves two purposes so far. First, as related to the previous discussion of nucleating domains using variable charges or electric fields, this work places a lower limit on how small the resulting nuclei can be and still be of use for switching.

Second, we will examine the effects of changing the background dielectric constant of the material. The background dielectric constant governs the electric fields that result from bound charges such as uncompensated domain walls, as previously described in Part 1:

$$\nabla^2\phi = \frac{-\rho_b}{\varepsilon_0\varepsilon_b}$$

By varying ε_b, we can vary the amount of depolarization fields created inside a nucleus. This serves as a proxy for examining the role of mobile charge, which would increase nuclei stability by the same mechanism, the reduction of the depolarization fields. [22]

5.2.1 Methods

We introduce a circular nucleus of radius r into a homogeneous, single domain of $+P_3$ using the *tanh* function:

$$P_3(x) = P_s tanh\left(\frac{||x-x_0||-r}{\xi}\right)$$

where x_0 is the reference location of the center of the nucleus, ξ governs the transition width, and P_s is the spontaneous polarization. In the case of $LiTaO_3$, $P_s \approx 0.5$ C/m^2. The nucleus polarization is aligned with the applied electric field.

We adopt somewhat flexible standards in determining what constitutes a "stable" nucleus. In nature, no nucleus should be stable under an applied field; at best, it would be metastable, either growing or shrinking over time. However, because of the roots of its formulation, the phase-field method typically represents a smoothed version of reality, and domains are less easily pinned in simulation that in experimental observation. At the same time, numerical constraints add some artificial pinning behavior back in, particularly if the numerical integration scheme is low-order in space or the resolution is relatively low (which it is, here).

With these in mind, we employ the same timestep size as above, and allow the simulation to run for a comfortably long period of time (3000 time steps), or until the nucleus has either shrunk by $> 50\%$, grown by $> 400\%$, or reached half the simulation volume. So long as the nucleus does not shrink to less than half its original size within the allotted time, it is deemed 'stable'. Typically

there is little change in the domain size after 1000 timesteps, so we feel that 3000 timesteps is justified and safe.

If a nucleus of size r is not stable, we increase r by 5% and try again, repeating until we find an approximation for the minimum stable nucleus. Here, we examine a range of electric fields from $0.1E_c$ to E_c, in increments of $0.1E_c$. For these simulations, we decreased the system size to 300nm x 300nm; otherwise, the parameters used here are the same as in Part 1.

5.2.2 Results

In Figure 5.6, we demonstrate the results across a range of applied electric fields for two different values of ε_b. Before discussion, we would like to refer the reader again to the discussion on $LiTaO_3$ background dielectric constants in Chapter 2, noting that the ε_b used here may be 3-4x too high, resulting in an inversely decreased electric field. However, adjusting ε_b here can still give us a qualitative idea of the effect of the charge screening.

As expected, we note that the stable nuclei size decreases with decreasing depolarization field. We also note an interesting shift between about $0.2E_c$ and $0.5E_c$, in which the minimum nuclei size drops sharply with increasing E_a before staying relatively constant. We postulate that this indicates a transition in the dominant energy form governing the nuclei size. When the applied field is low and the nuclei small, the depolarization fields inside the domain are too great, requiring a very large domain in order to separate the charges far enough that the resulting depolarization field is relatively low. As the applied field becomes larger, it compensates for increasing amounts of the depolarization field, allowing the minimum nuclei size to decrease and the bound charges to come closer together.

Once E_a is high enough that the depolarization field is sufficiently compensated, the Landau and gradient energy contributions dominate the nuclei size via their contribution to the domain wall energy.

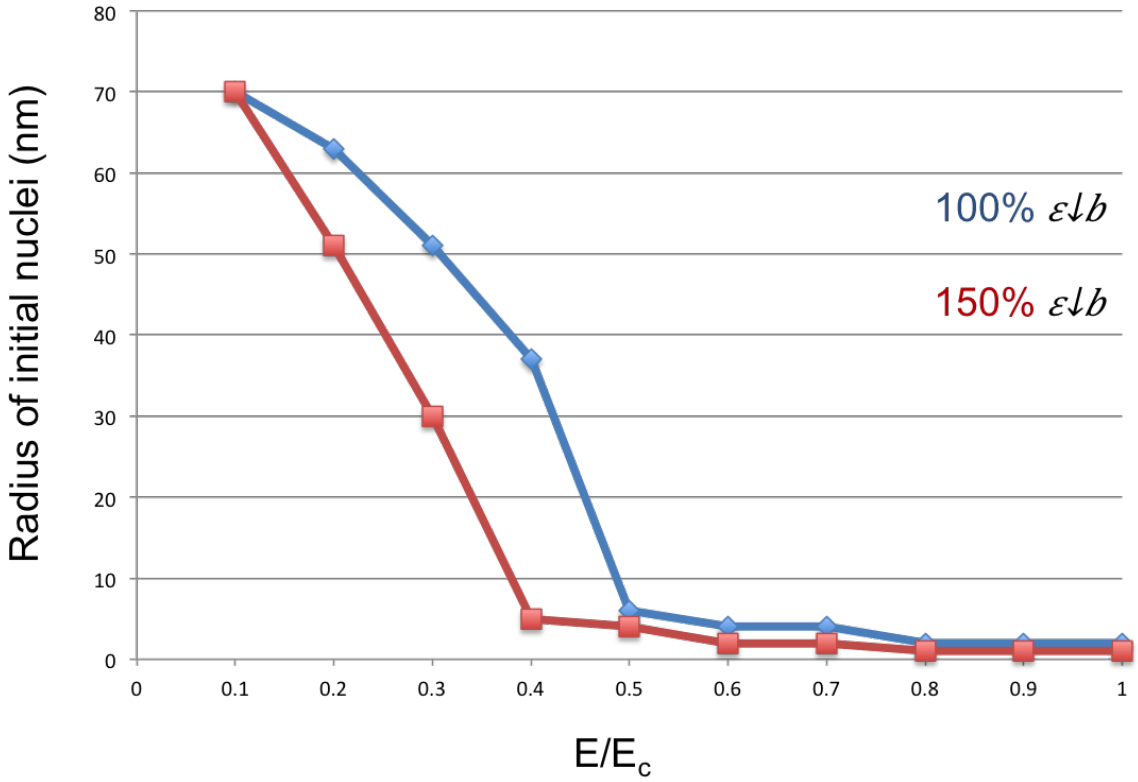

Figure 5.6. Minimum size of stable nuclei vs applied field, showing also the effect of changing the background dielectric constant, ε_b, which sets the electric field resulting from bound charge (such as at uncompensated domain walls). A larger ε_b means smaller resulting electric fields, and smaller stable nuclei.

Chapter 6

Conclusions

The primary goal of this work was to develop a better understanding of the processes and critical parameters associated with the formation and stability of nuclei of inverse-polarity ferroelectric domains within a matrix of homogeneous polarization, both to investigate mechanisms proposed to explain earlier experimental work and to guide future projects interested in controlling the highly nonlinear response of ferroelectric materials during the switching process. For example, as discussed in more detail in Reference [1], reliable operation of high power ferroelectric opening switches will require control of dynamic ferroelectric domain response to large electric fields. While not necessarily unexpected, quantifying the effects of mechanical damage on nucleation and switching behavior is important for cases in which surface-initiation of ferroelectric switching is sufficient or desirable. The most important contribution of this work, however, is in elucidating the mechanisms by which optically-assisted nucleation can occur. Certainly, there is still a need for better material parameter inputs before the model developed as part of this work can be fully predictive, but even the limited results produced so far are valuable for the associated physical and mechanistic insights into the relative magnitudes of the contributions from direct optical (electric) fields and screening effects of free charges. This work introduced a new phase-field capability to SNL while providing valuable insight into the mechanisms associated with mechanical and optical effects on nucleation for ferroelectric polarization reversal.

References

[1] G. L. Brennecka, F. J. Zutavern, G. J. Dension, M. B. Sinclair, M. A. Blea-Kirby, G. E. Peña, and S. F. Glover. "Controlled Polarization Reversal for Ferroelectric Opening Switches." [SAND2013-10422] (2013).

[2] W. J. Merz. "Domain Properties in $BaTiO_3$." *Phys. Rev.*, **88** [2] 421–422 (1952).

[3] W. J. Merz. "Domain Formation and Domain Wall Motion in Ferroelectric $BaTiO_3$ Single Crystals." *Phys. Rev.*, **95** [3] 690–698 (1954).

[4] R. Landauer, D. Young, and M. Drougard. "Polarization Reversal in the Barium Titanate Hysteresis Loop." *Journal of Applied Physics*, **27** [7] 752–758 (1956).

[5] R. Landauer. "Electrostatic Considerations in $BaTiO_3$ Domain Formation during Polarization Reversal." *Journal of Applied Physics*, **28** [2] 227–234 (1957).

[6] V. Gopalan and T. E. Mitchell. "Wall velocities, switching times, and the stabilization mechanism of 180° domains in congruent $LiTaO_3$ crystals." *J. Appl. Phys.*, **83** [2] 941–954 (1998).

[7] V. Gopalan, Q. Jia, and T. E. Mitchell. "*In situ* video observation of 180° domain kinetics in congruent $LiNbO_3$ crystals." *Appl. Phys. Lett.*, **75** [16] 2482–2484 (1999).

[8] V. Gopalan, S. S. A. Gertsl, A. Itagi, T. E. Mitchell, Q. Jia, T. E. Schlesinger, and D. D. Stancil. "Mobility of 180° domain walls in congruent $LiTaO_3$ measured using real-time electro-optic imaging microscopy." *J. Appl. Phys.*, **86** [3] 1638–1646 (1999).

[9] K. Fujimoto and Y. Cho. "High-speed switching of nanoscale ferroelectric domains in congruent single-crystal $LiTaO_3$." *Appl. Phys. Lett.*, **83** [25] 5265–5267 (2003).

[10] J. Li, B. Nagaraj, H. Liang, W. Cao, C. H. Lee, and R. Ramesh. "Ultrafast polarization switching in thin-film ferroelectrics." *Appl. Phys. Lett.*, **84** [7] 1174–1176 (2004).

[11] A. Gruverman, B. J. Rodriguez, C. Dehoff, J. D. Waldrep, A. I. Kingon, R. J. Nemanich, and J. S. Cross. "Direct studies of domain switching dynamics in thin film ferroelectric capacitors." *Appl. Phys. Lett.*, **87** 082902 (2005).

[12] A. Grigoriev, D.-H. Do, D. M. Kim, C.-B. Eom, B. Adams, E. M. Dufresne, and P. G. Evans. "Nanosecond Domain Wall Dynamics in Ferroelectric $Pb(Zr,Ti)O_3$ Thin Films." *Phys. Rev. Lett.*, **96** 18706 (2006).

[13] B. D. Huey, R. N. Premnath, S. Lee, and N. A. Polomoff. "High Speed SPM Applied for Direct Nanoscale Mapping of the Influence of Defects on Ferroelectric Switching Dynamics." *J. Am. Ceram. Soc.*, **95** [4] 1147–1162 (2012).

[14] L. Q. Chen. "Phase-Field Method of Phase Transitions/Domain Structures in Ferroelectric Thin Films: A Review." *Journal of the American Ceramic Society*, **91** [6] 1835–1844 (2008).

[15] M. Marvan and J. Fousek. "Electrostatic Energy of Ferroelectrics with Nonhomogeneous Distributions of Polarization and Free Charges." *Physica Status Solidi (B)*, **208** [2] 523–531 (1998).

[16] D. Scrymgeour, V. Gopalan, A. Itagi, A. Saxena, and P. Swart. "Phenomenological theory of a single domain wall in uniaxial trigonal ferroelectrics: lithium niobate and lithium tantalate." *Phys. Rev. B*, **71** [18] 184110 (2005).

[17] S. Kim, V. Gopalan, and B. Steiner. "Direct x-ray synchrotron imaging of strains at 180° domain walls in congruent $LiNbO_3$ and $LiTaO_3$ crystals." *Applied Physics Letters*, **77** [13] 2051–2053 (2000).

[18] T. Jach, S. Kim, V. Gopalan, S. Durbin, and D. Bright. "Long-range strains and the effects of applied field at 180° ferroelectric domain walls in lithium niobate." *Phys. Rev. B*, **69** 064113 (2004).

[19] K. Hassani, M. Sutton, M. Holt, Y. Zuo, and D. Plant. "X-ray diffraction imaging of strain fields in a domain-inverted $LiTaO_3$ crystal." *Journal of Applied Physics*, **104** 043515 (2008).

[20] Y. Ishibashi and Y. Takagi. "Note on Ferroelectric Domain Switching." *J. Phys. Soc. Jpn*, **31** [2] 506–510 (1971).

[21] Y.-H. Shin, I. Grinberg, I.-W. Chen, and A. Rappe. "Nucleation and growth mechanism of ferroelectric domain-wall motion." *Nature*, **449** 881–884 (2007).

[22] A.-Q. Jiang, H. Lee, C. Hwang, and T.-A. Tang. "Resolving the Landauer paradox in ferroelectric switching by high-field charge injection." *Phys. Rev. B*, **80** [2] 024119 (2009).

[23] J. Fousek, M. Marvan, and R. Cudney. "Localized switching in photorefractive ferroelectrics induced by spatially inhomogeneous electric fields." *Applied Physics Letters*, **72** [4] 430 (1998).

[24] C. Sones, M. Wengler, C. E. Valdivia, S. Mailis, R. W. Eason, and K. Buse. "Light-induced order-of-magnitude decrease in the electric field for domain nucleation in MgO-doped lithium niobate crystals." *Appl. Phys. Lett.*, **86** 212901 (2005).

[25] C. Sones, A. Miur, Y. Ying, S. Mailis, R. W. Eason, T. Jungk, A. Hoffman, and E. Soergel. "Precision nanoscale domain engineering of lithium niobate via UV laser induced inhibition of poling." *Appl. Phys. Lett.*, **92** 072905 (2008).

[26] K. Buse. "Light-induced charge transport processes in photorefractive crystals I: Models and experimental methods." *Applied Physics B: Lasers and Optics*, pages 273–291 (1997).

[27] K. Buse. "Light-induced charge transport processes in photorefractive crystals I: Materials." *Applied Physics B: Lasers and Optics*, pages 391–407 (1997).

Appendix A

Material parameters for $LiTaO_3$

The following material parameters were drawn from reference [16] and are used in the simulations descried herein:

Table A.1. Landau Parameters (in 10^9 Nm^2/C^2)

α_1	1.11
α_3	-0.628
α_{33}	1.261

Table A.2. Elastic stiffness tensor components (in 10^{11} N/m^2)

c_{11}	2.3305
c_{12}	0.4644
c_{13}	0.8358
c_{33}	-2.7414
c_{14}	-1.067
c_{44}	0.9526

The electrostrictive tensor components are assumed to be zero (see phenomenological theory discussion). The background (static) dielectric constant (relative permittivity) is assumed to be isotropic and equal to a value of $\varepsilon_{b,11} = \varepsilon_{b,22} = \varepsilon_{b,33} = 45$. Similarly, the gradient energy coefficient is also assumed to be isotropic, such that $g_{11} = 2g_{44} = 2g'_{44}$, and $g_{12} = 0$. Finally, the kinetic coefficient L is implicitly taken to be 1.

DISTRIBUTION:

1	MS 0828	Steven N. Kempka, 1510
1	MS 1152	Steve F. Glover, 1353
1	MS 1181	Larry X. Schneider, 1350
1	MS 1411	Geoff L. Brennecka, 1816
1	MS 1411	Paul G. Clem, 1816
1	MS 1411	Amy C. Sun, 1814
1	MS 1411	Ben M. Winchester, 1814
1	MS 0899	Technical Library, 9536 (electronic copy)

Sandia National Laboratories